PNAS Nexus, 2024, 3, pgae514
https://doi.org/10.1093/pnasnexus/pgae514
Advance access publication 15 November 2024
Research Report

Infiltration depth, rooting depth, and regolith flushing—A global perspective

Ying Fan [a,*] and Gonzalo Miguez-Macho [b]

[a]Department of Earth and Planetary Sciences, Rutgers University, New Brunswick, NJ 08544, USA
[b]CRETUS, Non-Linear Physics Group, Faculty of Physics, Universidade de Santiago de Compostela, Galicia 15782, Spain
*To whom correspondence should be addressed: Email: yingfan@eps.rutgers.edu
Edited By Barbara Romanowicz

Abstract

In the vegetation root zone, infiltration (*Inf*) parts in two directions with distinct Earth-system functions. One goes up as evapotranspiration ($E + Tr$), returning *Inf* to the atmosphere (short-circuiting) and affecting short-term weather/climate and the carbon cycle. The other goes down as deep drainage (*DD*), flushing the regolith, mobilizing nutrients/contaminates and dissolved minerals into aquifers and rivers, eventually reaching the ocean (long-circuiting) thus regulating global biogeochemical cycles and long-term climate. We ask, what is the modern-day global structure in short- vs. long-circuiting? What forces and feedbacks create such structures? Synthesizing site-studies aided by global modeling, we found that: (i) long-circuiting prevails in evenly wet climates, in well-drained landscapes with a deep vadose zone, in substrates with deep conduits, and with plant biomass below natural equilibrium; (ii) soil B-horizons, via geochemical and vegetation feedbacks, enhance short-circuiting, while deep rock fractures enable long-circuiting even in dry climates; (iii) in dry climate/season and in uplands, plant roots follow *Inf* into deep vadose zone to tap wet-season *Inf*; (iv) plant water-use reinforces shallow *Inf*, reducing *DD* and regolith flushing in dry and season-dry climates; (v) where short-circuiting prevails, a dry soil zone separates modern surface processes from fossil groundwater; and (vi) the $E + Tr$ supply depth, regolith flushing rate, and groundwater residence time vary greatly across the land, arising from multiscale drivers/feedbacks among climate, drainage, substrate, and biomass. These findings link site-based process discoveries to Earth-system level structures and functions of water belowground, shedding light on where/when/how the infiltrated rain influences the atmosphere above or the ocean downstream.

Significance Statement

How deep does the rain regularly infiltrate into the ground? Do plant roots follow? How much infiltration is pumped back to the atmosphere and how much passes below plant roots reaching the water table, flushing the regolith, recharging aquifers and rivers, and eventually reaching the ocean? What is the depth that supplies evapotranspiration, and what is the regolith flush rate? What are the implications to global material and energy cycles? The answers depend on local climate–terrain–vegetation combinations. We shed mechanistic light on multiscale causes–feedbacks among climate, drainage, substrate, and plant biomass that interactively create a global structure in the depths and rates of hydrologic plumbing of the Earth's critical zone, informing global models on critical depths and processes to include in Earth-system predictions.

Introduction

Figure 1A schematically illustrates the hydrologic pathways after precipitation (*P*) falls on a hillside. We focus on the fluxes in the vadose zone (filled arrows), the unsaturated soil–saprolite–rock column from the land surface to the water table (*WT*). Here the infiltration (*Inf*) from *P* parts in two directions, one as soil evaporation (soil *E*) plus root-uptake for plant transpiration (plant *Tr*) returning *Inf* to the atmosphere as $E + Tr$, and the other as deep drainage (*DD*) reaching *WT* (perched or anchored) and hence streams via shallow or deep paths, eventually terminating in coastal oceans or inland seas. If *Inf* returns to the atmosphere in situ, it is "short-circuited" (in dashed red circle). If *Inf* reaches the local *WT* and the streams, it follows the "long circuit" (in solid red circle) with longer flow paths and residence times on land.

We contrast short- vs. long-circuiting because they perform distinct functions in the Earth's critical zone, the biogeochemically activated upper continental crust (1–4). Where short-circuiting prevails, *Inf* regulates land-to-atmosphere mass/energy fluxes, affecting short-term weather/climate and land ecosystem productivity; but only shallow depths are wetted, habitable, and reactive; the respired soil CO_2 diffuses back to the atmosphere; weathering products stay on land; and the groundwater receives little recharge and is hence disconnected from modern surface

Competing Interest: The authors declare no competing interests.
Received: July 8, 2024. **Accepted:** November 4, 2024

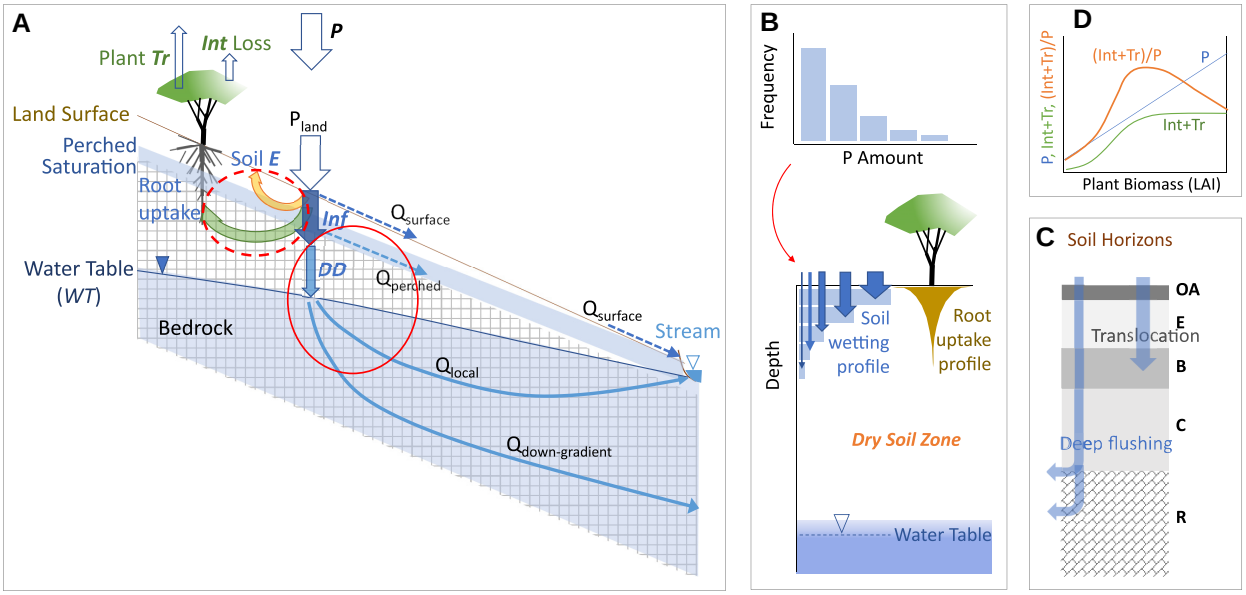

Fig. 1. A) Schematic of the fate of *P* fallen on a hillside: canopy interception and loss to evaporation (*Int* loss), *P* reaching land surface (P_{land}), and its partition to surface runoff ($Q_{surface}$) and *Inf* into the subsurface. $Q_{surface}$ can occur as both infiltration- and saturation-excess runoff (near the valley). We focus on the fate of *Inf* in the vadose zone (filled arrows). *Inf* branches into four paths: soil water evaporation (soil *E*), root-uptake for Plant *Tr*, shallow flow in perched saturated zone during *P* or melt events entering local streams ($Q_{perched}$, interflow, stormflow), and *DD* that "escapes" root-uptake and reaches the permanent *WT*, from which it discharges into local (Q_{local}) or down-gradient streams ($Q_{down\text{-}gradient}$, underflow) through deeper flow paths. Fluxes within the red dashed circle are referred to as "short-circuiting", and those in the red solid circle as "long-circuiting". B) (Top) A common feature in *P* amount-frequency distribution with more frequent small events, particularly in drier climates; (Bottom) the skewed *P* distribution leads to a skewed wetting depth distribution with more frequent shallow wetting, which is exacerbated by *E* + *Tr* consuming earlier *Inf*, preventing the cumulative deepening of the wetting front; the frequent shallow wetting leads to frequent shallow root water-uptake, and in water-stressed systems rooting depths follow *Inf*-depths; a dry soil zone may exist where all *Inf* is consumed by *E* + *Tr*, separating modern-day surface processes from the deep fossil groundwater. C) Schematic of a soil–saprolite–rock column with well-developed soil horizons, where "translocation" leaches the OA-E horizons and deposits the leached material in the B-horizon, resulting in lower permeability in the latter, impeding *Inf*, enhancing water holding capacity of shallow soils for *E* + *Tr* and reducing *DD*. D) Hypothesized vegetation impact on *DD*, as (*Int* + *Tr*)/*P* ratio along biomass gradient, in a hump-shaped curve with the greatest vegetation impact in semiarid and season-arid biomes where vegetation consumes the largest proportion of *P*.

processes. Where long-circuiting prevails, the entire regolith column is regularly wetted, habitable, and reactive; the respired soil CO_2 acidifies *DD* enhancing chemical weathering and creating porosity (5); and solutes are flushed into streams (6) and the ocean, completing the land phase of global biogeochemical cycling; the groundwater is recharged feeding steady streamflow, but nutrients are leached and contaminants mobilized into aquifers and aquatic habitats. Such distinct functions of short- vs. long-circuiting prompt some basic questions: Across the land today, where does long-circuiting prevail and where is short-circuiting the norm? What forces and feedbacks create such patterns? What are the implications for global material cycling and change?

The answers hinge on *Inf*-depth and its frequency and amount passing below the plant root zone to "escape" uptake and continue downward. Intuitively, anywhere on land, *Inf*-depth depends on *P*-supply minus *E* + *Tr* demand (the climate driver) yielding surplus for *DD*; it depends on substrate properties (terrain driver) affecting *Inf* rate/depth; it depends on the plant biomass and rooting-depth (vegetation driver) setting *Tr* demand and uptake depth. We thus explore climate, terrain, and vegetation as primary but interactive drivers. We test six hypotheses from global to plot scales. Some are obvious such as wetter climates allow deeper *Inf*, but they are included to systematically explore patterns arising from multiple drivers at multiple scales that create a global tapestry not explained by a single driver alone.

H1—Climate: At global–regional scales, *Inf*-depth broadly reflects the climate for many reasons. (i) In wetter climates, *Inf* exceeds *E* + *Tr* demand leaving surplus to percolate deeper, while in arid climates, the low annual *P* and high frequency of small, isolated pulses (Fig. 1B, top) wet only shallow depths, and *E* + *Tr* during the long dry spells consume earlier *Inf* preventing the cumulative advance of wetting fronts. (ii) Climate strongly controls plant biomass hence *Tr* demand. Lastly but importantly, (iii) climate controls the sensitivity of *Inf* and *DD* to local drivers as detailed in H2–H6 below, whereby the mechanisms and impacts of drainage, substrate, and vegetation response/feedback all depend on climate.

H2—Drainage: At regional–landscape scales, *Inf*-depth differs between well-drained uplands with a deep vadose zone and poorly drained lowlands with a shallow *WT*. The mechanisms depend on the climate and the season. (i) In humid climate/season with potentially deep *Inf*, it is deeper in uplands with a deeper vadose zone, and shallower in lowlands with a shallow *WT* that truncates *Inf*. (ii) In dry climates/seasons, runoff into lowlands adds to local *P*, potentially deepening *Inf*, but higher valley biomass (e.g. riparian forests) and *E* + *Tr* consume the added input preventing deeper *Inf*. Furthermore, a shallow valley *WT* can be tapped by *E* + *Tr*, yielding net upward flux (−*DD*) sustained by +*DD* in uplands (7, 8) or wetter times (7). Such returns of upland/past *DD* to the atmosphere, after having escaped *E* + *Tr* before, form patches of "−" *DD* in arid basins, flushing solutes upward and depositing inland evaporites.

H3—Substrate: At landscape–plot scales, the structure of the soil–saprolite–rock column exerts primary controls on *Inf* and *DD*. A coarse-textured surface allows easy *Inf* entry but the

terminal *Inf*-depth depends on the deeper barriers/conduits. For example, a soil B-horizon (Fig. 1C), formed by *Inf* terminating and depositing/reprecipitating leachates from above, can impede *DD*; and by holding up *Inf* to be used by $E + Tr$ long after rain (9, 10), it further reduces *DD*. For another example, upland shallow bedrock can impede deep *Inf* causing perched stormflow (11, 12) ($Q_{perched}$, Fig. 1A). However, shallow bedrock is commonly fractured under topographic (13) or tectonic (14) stress, and feedbacks with infiltrating water at longer timescales, particularly in carbonates (15), can create efficient conduits channeling fast/deep *Inf* (16–18) to reach *WT* and enter streams via groundwater flow paths (Q_{local}, $Q_{down\text{-}gradient}$, Fig. 1A). Such preferential flow, via fractures or macropores, is a key mechanism for deep *Inf*, making it possible even in arid climates (15, 19, 20). Deep *Inf* can also be achieved in deeply weathered upland tropical and temperate soils with a thick vadose zone (21). However, in all scenarios of deep *Inf*, deep-rooted plants can "pull it back" in dry times (18, 21) (see H4), so that deeper *Inf* does not necessarily lead to higher *DD*.

H4—Vegetation response: Where water is limiting, plant rooting depths follow *Inf*-depths (22, 23) (Fig. 1B, bottom), pulling back deep moisture in dry times that is filled in wetter times (18, 24). In ecosystems relying on recycled nutrients from standing biomass, wetting depths set microbial life hence nutrient-release depths (25) and nutrient-leaching depths, thus indirectly shaping the root profile (26). However, rooting-depth decouples from *Inf*-depth in the following situations: (i) In per-humid climates where water is not limiting, (ii) in lowlands where a shallow *WT* restricts roots to the aerated soils above it, (iii) in arid valleys where the local *Inf* is superficial, but a deeper *WT*, fed by regional flow, is accessible to roots, pulling the roots deeper than *Inf*-depths (27), and (iv) where the introduced vegetation demands more (28) or less (29) water than the local climate and soil storage can provide. But under arid-semiarid and season-arid climates, on uplands free of *WT* influence, root-uptake depths adapt to *Inf*-depths, allowing plants to maximize *Inf* use under water stress, often consuming it all in dry biomes.

H5—Vegetation feedback: By uptaking water between *Inf*-events, vegetation "resets" the soil profile to dry "initial conditions" for later *Inf* pulses, which must fill the shallow deficits and "prime" soil hydraulic conductivity before advancing deeper. Hence, plant water-use reinforces and perpetuates shallow *Inf* (feedback). The feedback strength depends on plant biomass affecting canopy interception (*Int* loss) and *Tr* (Fig. 1A). The plant impact on the effective *P* available for *DD*, or the $(Int + Tr)/P$ ratio (Fig. 1D), should be low in arid biomes with negligible biomass, increase in semiarid, and peak in season-arid biomes with an increasing biomass consuming larger portions of *P*, and decline in humid biomes where *P* exceeds $E + Tr$ demand yielding increasing surplus for *DD*. Thus the vegetation impact on *DD* is nonlinear and takes a hump-shape (30) (Fig. 1D). Vegetation can indeed enhance *Inf* by allowing runon to infiltrate (31, 32) and by canopy–stem–root funneling (33), aided by biogenic macropores (34, 35). But the *Inf*-gain must come after *Int*-loss, and evidence suggests that, in dry ecosystems, vegetation-induced deeper *Inf* is consumed by the vegetation itself (36), with the end result of reduced *DD* (37).

H6—Dry soil zone: Where short-circuiting prevails today, a dry soil zone (Fig. 1B) forms between root-uptake depth and *WT* capillary rise. This dry zone is substantial in arid uplands where the superficial *Inf* is entirely consumed by $E + Tr$. It thins downslope due to a thinner vadose zone over a shallower *WT*. It is absent where rock fractures provide efficient vertical conduits. It thickens under the introduced higher biomass (28, 38, 39) that taps progressively deeper reserves filled in the past. Finally, it is highly sensitive to biomass in semiarid and season-arid climates. This dry zone severs the hydraulic and biogeochemical connection between modern surface processes and the deep fossil groundwater, and it indicates areas on Earth where the land only exchanges mass and energy with the atmosphere above but contributes little toward freshwater and geochemical export to the oceans downstream.

Materials and methods

We test these hypotheses following two complementary approaches: (i) synthesis of site observations to gain mechanistic insights and (ii) global hydrologic model simulation to explore large-scale structures.

Synthesis of site-based observations

We reviewed published site-studies to understand site-specific complexities in a global context, searching for common climate–terrain–vegetation threads. These site-studies pertain to a wide range of timescales using a variety of methods (Table S1), including one-time trenching/coring/penetrometers after *P* events, event-seasonal *DD* flux with lysimeters, subdaily soil water monitoring at multiple depths over full or multiple seasons, shallow upland *WT* response to *P* events/seasons, cave ceiling drip, time-lapse section- and borehole- geophysics, and various chemical tracers (dye, O/H isotopes, $^{-}$Cl, ^{3}H). Generally, *Inf* inferred from events is shallower than from seasons, which is shallower than from tracers, the latter reflecting long-term cumulative *Inf*, particularly in arid climates. Many studies did not reach the terminal *Inf*-depth, so the compiled values are biased shallow.

We focus on seasonal dynamics, recording seasonal maximum *Inf*-depth, *DD* frequency and amount over annual climate and plant-growth cycles, to avoid ambiguity in tracking events yet resolve a fundamental rhythm in Earth's energy/material cycling. Seasonal maximum *Inf*-depth is recorded as the deepest depth of moisture increases in a year averaged over multiple years if available. Seasonal *DD* frequency is the number of months per year when *Inf* reaches below reported rooting depths, divided by 12 months, and *DD* amount is the annual downward flux (mm/year) below the root zone (see Section S1). Results are shown in Fig. 2 at 509 plots from 194 studies. Our review is not exhaustive but intended to sample a wide range of climate–terrain–vegetation conditions.

Global hydrologic modeling

We use a global hydrology and root-uptake model (7, 27) called ASAP (as simple as possible) to (i) track *Inf*, *E*, *Tr*, and *DD* flux separately which is difficult by observations and (ii) explore global patterns across climate–terrain–vegetation settings not fully sampled by site-studies. Details of the model are given in Section S2. Briefly, it is built on global 30″ (~1 km) grids to resolve upland-to-lowland drainage within storage-computation limits, computed hourly for 15 years (2003–2018) to capture event, seasonal, and interannual dynamics. ASAP has two main modules (Fig. S1): (i) the hydrology module solving Richards' equation in the vadose zone, Darcy's law for 2D groundwater flow and two-way groundwater–river/floodplain exchange, forced by climate reanalysis, soil and topography from global datasets (Table S3). A grid column has 40 resolved layers in the top 1 km depth (Table S2), but porosity and permeability continue below 1 km. These material properties are parameterized to decrease

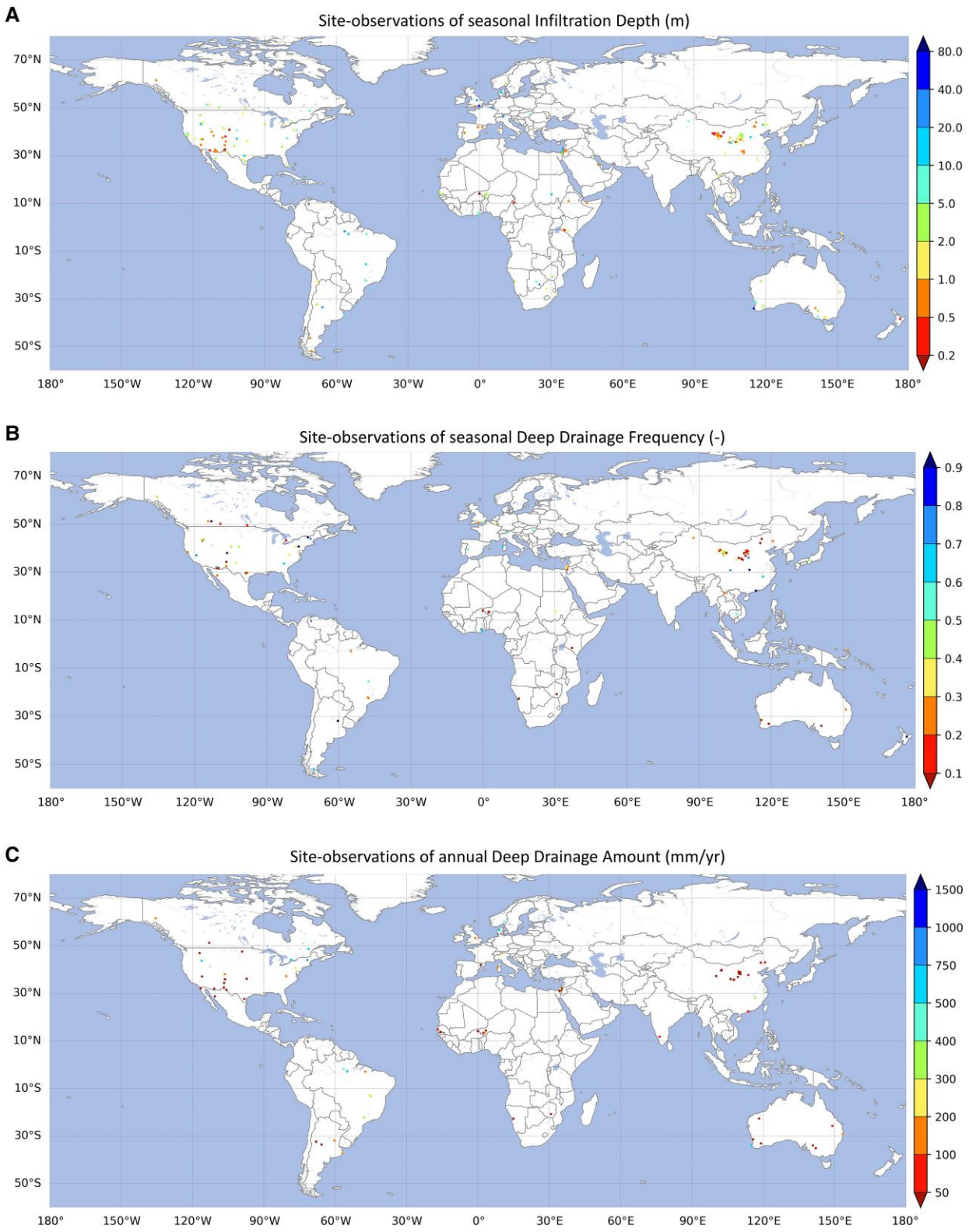

Fig. 2. The 509 sites of 194 studies from the published literature reporting *Inf*-depth, *DD* frequency, and amount using a variety of field methods (Table S1): A) seasonal maximum *Inf*-depth (m) over an annual cycle; B) seasonal *DD* frequency, calculated as the number of months per year when *Inf* reached below plant rooting-depth, divided by 12; and C) annual amount of *DD* recharge (mm/year); all three variables are averaged over multiple years where available. Many studies investigated multiple sites within a small area and they appear on top of one another, with the values seen reflecting the order of plotting. Please consult the data table to see the high local variability in each of these variables.

exponentially with depth from the values in the top 1 m based on global datasets. However, to reflect the large difference in regolith thickness across the world, we let the exponential decrease rate (e-folding depth) depend on land slope (40), yielding shallow regolith on steep slopes but deep sediment in flat basins (Fig. S2). It is also shallow in cold regions to mimic the frost barrier (41).

This module gives hourly *Inf*, *DD*, *WT*-depth, groundwater discharge to streams or stream leakage to riverbed/floodplain sediments in each grid-cell, and groundwater and streamflow among grid-cells. The dynamic soil water profiles, wetted from the top by *Inf* and below by *WT*, set the stage for plant root-uptake. (ii) The plant root-uptake module, calculating *Tr* by Penman–Monteith equation driven by satellite biomass (leaf area index, *LAI*) and reanalysis air vapor pressure deficit, giving plant water use that must be met by root-uptake. This model-inverted plant water use (7) is then allocated among soil layers following Ohm's law so that uptake favors wetter and shallower soils (Fig. S3).

Modeled monthly fluxes are compared with $E + Tr$ at 103 flux-tower sites (42) (Figs. S4 and S5, Table S4) and stream flow at 34 gauges (Fig. S6). Without calibration to match flux-tower and river-gage observations, ASAP captures the seasonal water balance at flux-tower (~2 km footprint) and river-basin (~200 to >4 million km^2) scales. Discrepancies are largely caused by neglecting human activities such as irrigation affecting soil *E* and crop *Tr*, groundwater pumping, river diversion, and dams affecting streamflow. Being simple, the model neglects soil B-horizons and rock fractures, thus we will not use it to test H3 on substrates. Figure 3 shows the modeled seasonal *Inf*-depth, *DD* frequency, and amount (Section S2.8).

Results

We test the six hypotheses using the 509 site observations first followed by global model results, with supplementary results given in Section S3.

Regional climate (H1)

We test H1 that globally, a wetter climate leads to deeper *Inf* despite diverse site conditions. Figure 4A plots seasonal *Inf*-depth vs. mean annual *P*, separating winter-wet, summer-wet, and even-wet/dry sites. *Inf* generally deepens with higher *P* (statistics in Table S5), but at winter-wet sites, *Inf* is deeper under the same *P* and deepens faster with increasing *P*, as any additional *P* is more likely to pass below the winter $E + Tr$ depth. Figure S7 plots *DD* frequency and amount vs. *P*, showing that the deeper *Inf* at winter-wet sites did not result in a higher *DD*, likely because deep-rooted vegetation "pulled back" the winter-*Inf* in the dry summer. The highest *DD* is achieved in the more equitable climates (green).

Model results (Fig. 3) suggest a climate signal strongly modulated by drainage. For example, the shallowest *Inf* (Fig. 3A) is found in the large deserts of the world due to aridity, but also in the Amazon floodplain and arctic permafrost due to the shallow *WT*. The deepest *Inf* occurred in mountains, partly due to higher orographic *P* and focused snowmelt seasons, and partly due to an efficient drainage and a deep vadose zone that accommodates deep *Inf*, despite a shallower model regolith in mountains (Fig. S2). Patterns in *DD* (Fig. 3B and C) are dominated by climate; zero in deserts and highest in humid climates. But significant *DD* also occurs in arid river valleys and deltas such as the Nile, the Niger, and the Okavango (Fig. 3 inset, BW and BS climate), where the rivers are sourced in remote and wetter mountains. Table S6 tabulates the model results in Fig. 3. The hundreds of millions of grid-cells are grouped by 31 Köppen–Geiger climates (Fig. S8) and within a climate by upland vs. lowland for testing H2. Figure 5A–C plots the model *Inf* and *DD* vs. annual *P*. In drier climates ($P < 800$ mm/year, box), model *Inf* echoes site data (Fig. 4A), deepening with higher *P*, but the trend reverses with further increase in *P* due to increasing land saturation. As expected, *DD* frequency and amount increase with higher *P*, but with less scatter than site data (Fig. S7) as the model missed site-scale variations in substrate and vegetation, and the results are averaged over large climate zones.

Drainage (H2)

To test H2 on land-drainage effect, with *WT*-depth as an indicator of drainage conditions, we plot *Inf*- vs. *WT*-depth from site-studies (Fig. 4B). It shows that the *WT*-depth is the lower bound of *Inf*-depth; the points slightly below the 1:1 line are sites where large *WT* fluctuations result in a mean *WT* (plotted here) shallower than seasonal maximum *Inf*-depth. *Inf* terminates at *WT* (on 1:1 line) in humid (blue) but also arid climates (red–orange), the latter via deep conduits in karsts (15, 20). The drainage effect on *DD* is less clear (Fig. S9, Table S7) due to competing mechanisms: runoff into valleys potentially increases valley *DD*, but in a humid climate valley saturation prevents *DD*, and in an arid climate the higher valley $E + Tr$ also prevents *DD*. Thus in valley settings, the interplay among runoff input, saturation or higher $E + Tr$ loss, all varying across climate and season, determines if *DD* is higher or lower.

Model results (Fig. 3A) show a deeper *Inf* in better-drained uplands. This occurs at the continental (mountains vs. floodplains) to local (hills vs. valleys, insets, to the extent resolved by the ~1 km model grid) scales. This pattern is seen in Fig. 5A, with far shallower *Inf* in lowlands (filled squares), particularly in the high-*P* range with increasing valley saturation. Figure 5D–G further explores the *Inf*-*WT* relation in different climates and across the season, plotting monthly *Inf*- vs. *WT*-depth. It suggests that, first, in all climates and all months, *Inf* penetrated deeper in uplands (+) than lowlands (∇). Second, the drier the climate (ordered by the Köppen–Geiger climate class A–C–D–B), the larger the gaps between *Inf*- and *WT*-depths, so that in arid B climate, *WT*-depth is no longer a limiting factor for *Inf*-depth. However, although *Inf* does not reach *WT* seasonally, it can do so in wetter periods such as large cyclones and El Niño or La Niña years (43, 44).

Substrate structure (H3)

We test H3 that at local scales, the substrate structure exerts primary controls on *Inf* and *DD*. First, we plot *Inf*-depth and *DD* against the soil texture given by the site-studies (Fig. S10). *Inf*-depth varied over orders of magnitude for a given texture class, with no patterns in *DD* frequency and amount. The low correlation is partly explained by deeper barriers or conduits below surface soils. In Fig. 4C, *Inf*-depths correlate well with the soil B-horizon depths (Pearson $r = 0.80$, Table S8). It is no surprise as B-horizons are products of *Inf*; it is the depth where *Inf* ends, depositing/mineralizing leachates from above via translocation (Fig. 1C). The process reduces permeability and impedes *Inf*. Two feedbacks likely cemented the correlation: (i) a developing B-horizon impedes *Inf*, affirming its formation by more deposition, and (ii) by holding *Inf* longer above or within a developing B-horizon, it boosts plant root-uptake long after the rain (9), further reducing the surplus for deeper *Inf* and *DD*. In contrast, *Inf* did not always stop at the reported bedrock surface (Fig. 4D) but frequently penetrated below, because bedrock fractures are efficient conduits for deep *Inf*. This happened in wet or winter-wet climates (blue points below 1:1) but also in dry or summer-wet climates in karst terrain (orange points), highlighting the critical control of the substrate. To assess the impact of preferential flow via deep fractures or macropores, we plot

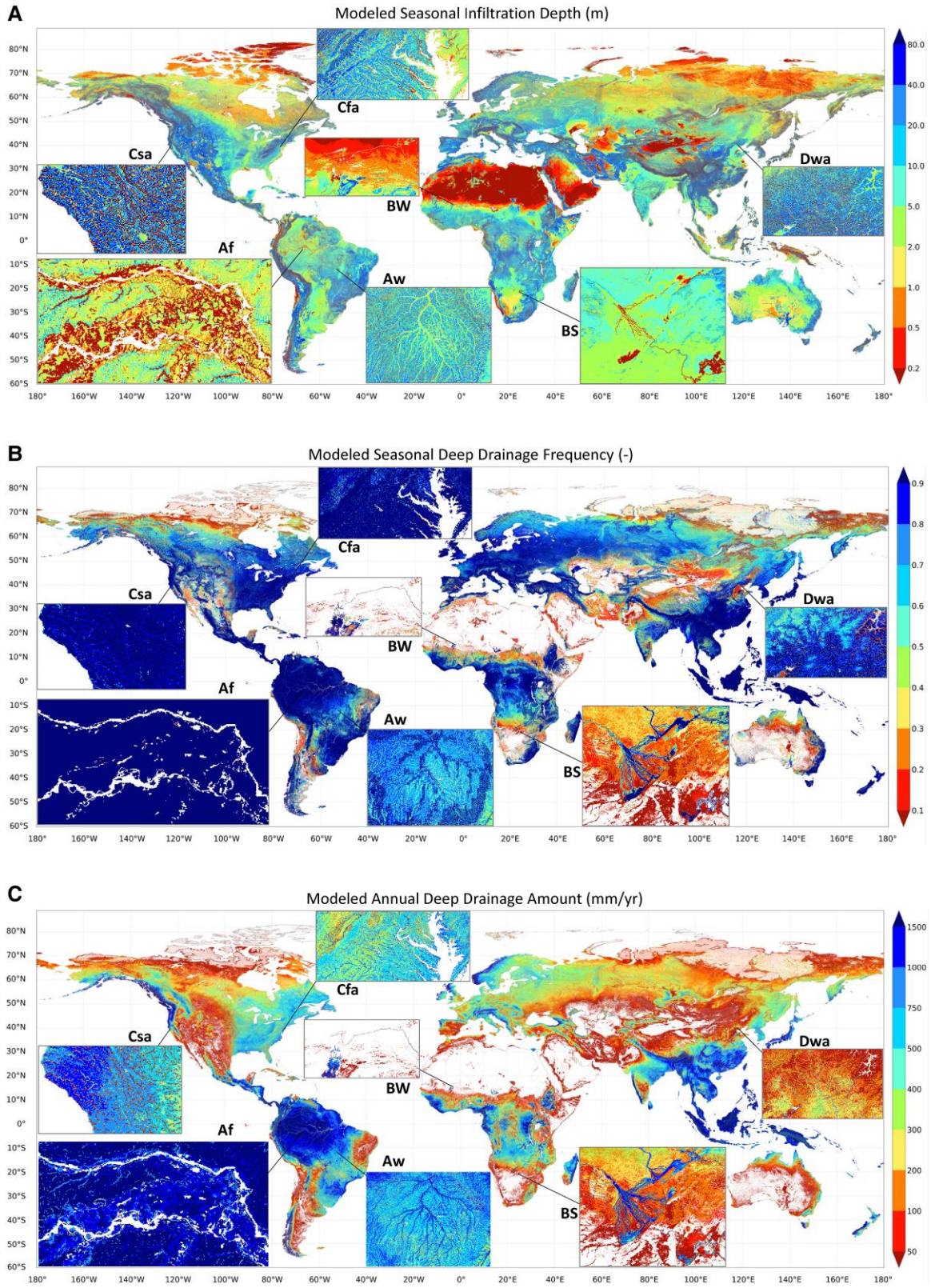

Fig. 3. A) Modeled seasonal *Inf*-depth (m), B) *DD* frequency as number of months per year when *Inf* reached below plant uptake depth divided by 12, and C) *DD* amount (mm/year). Blank = flux < 1 mm/year. See Section S2.8 for details on making these maps. Insets give local details for seven Köpen–Geiger climate classes: Af (tropical forest, humid), Aw (tropical savanna, winter-dry), BS (semiarid steppe), BW (arid desert), Cfa (temperate, humid, hot summer), Csa (temperate, summer-dry, hot summer), and Dwa (continental, winter-dry, hot summer).

Inf-depths vs. *P*, separating sites with and without reported evidence for preferential flow (Fig. S11a). Preferential flow (blue) deepened *Inf* by ~5 m across all climates, and *Inf*-depth distribution (Fig. S11b) suggests mostly shallow *Inf* without it. Because not all studies addressed the process of preferential flow, its role may be under-reported.

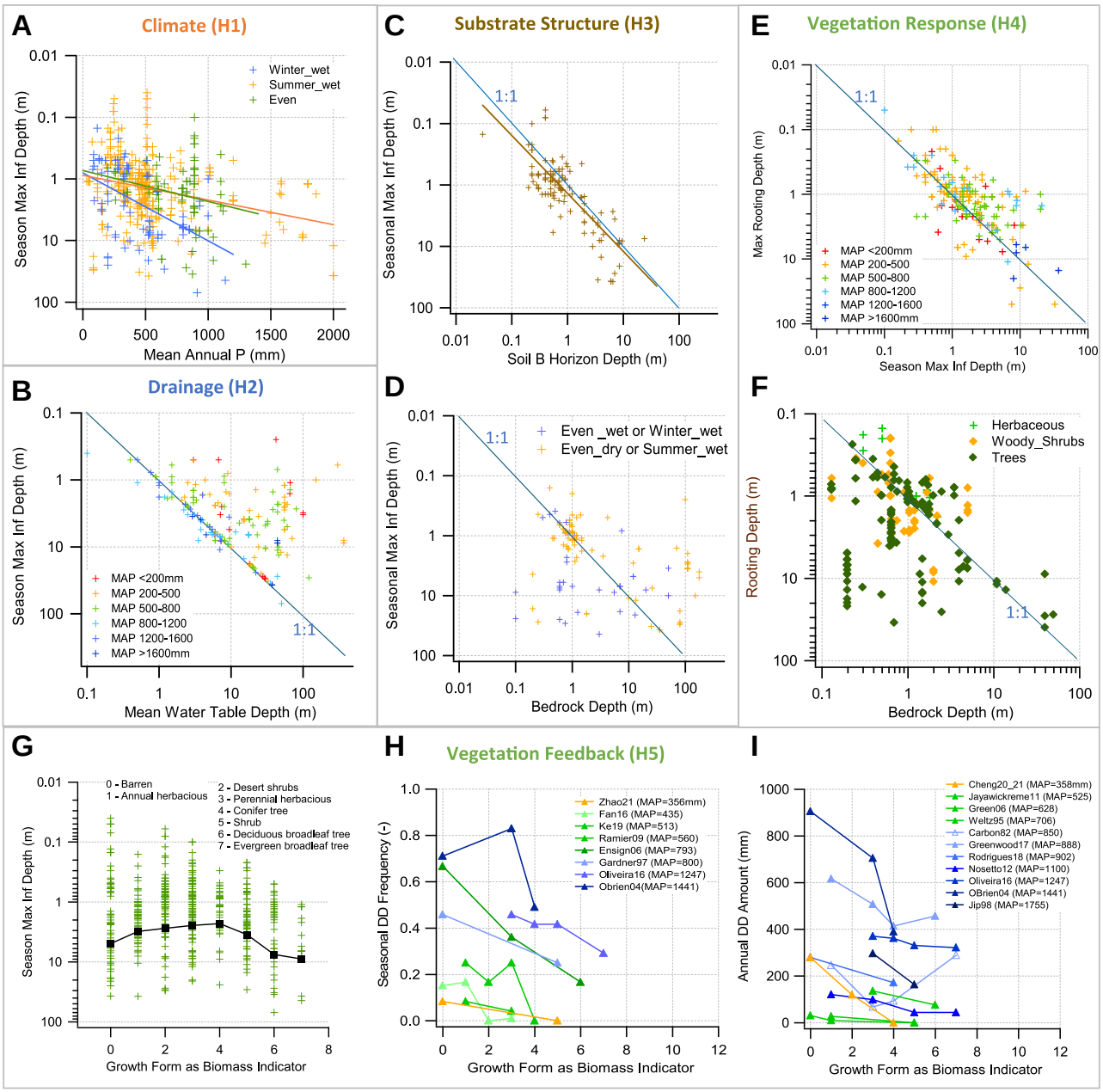

Fig. 4. Testing hypotheses H1–H5 with site observations. A) Climate (H1): *Inf*-depth vs. mean annual *P*, separating winter-wet, summer-wet, and even-wet/dry sites (statistics in Table S5). B) Drainage (H2): *Inf*-depth vs. *WT*-depth (statistics in Table S7). C, D) Substrate (H3): *Inf*-depth vs. soil B-horizon and bedrock depths (statistics in Table S8). E, F) Vegetation response (H4): rooting-depth vs. *Inf*-depth (statistics in Table S9) and bedrock-depth. G–I) Vegetation feedback (H5): *Inf*-depth vs. growth form as biomass indicator with class-mean as black squares, *DD* frequency and *DD* amount from site-studies with vegetation as the only variable across multiple sites under the same climate–terrain settings (legend show mean annual *P* in mm).

Vegetation response (H4)

We test H4 that in arid and season-arid uplands, plant rooting-depth is influenced by seasonal *Inf*-depth. We posed this hypothesis earlier (27) on hydrologic regulation of plant rooting-depth along climate and drainage gradients (Fig. S12). At that time, we lacked collocated root- and *Inf*-depth observations, and compiling that dataset was a primary motivation for this study. Figure 4E plots root- vs. seasonal *Inf*-depth, including all observations under all climate–drainage conditions. The results support H4 (Pearson $r = 0.65$, Table S9) despite including sites outside the hypothesized climate–drainage window (arid to season-arid, uplands without *WT* influence, cases 1 and 4 in Fig. S12). We numbered and analyzed the sites with the largest deviations from the 1:1 line (Fig. S13a, Table S10) confirming that they are indeed far from our hypothesized site conditions (see Discussion in Section S3.4). Further evidence of roots following deep *Inf* is found in Fig. 4F plotting root- vs. bedrock-depth (data from (27)). Points below 1:1 are roots tapping into rock fractures, all woody plants in strongly seasonal climates where the wet season fills the deep fractures and the dry season demands its use.

Figure 5H–K gives the model results, plotting monthly root-uptake vs. *Inf*-depths, grouped by the climate and separating uplands vs. lowlands (as in Fig. 5D–G). In arid B climate (Fig. 5I) on uplands (+), root-uptake depth followed *Inf*-depth (near 1:1 line), while in lowlands (∇), roots went below *Inf*-depth to tap the *WT*

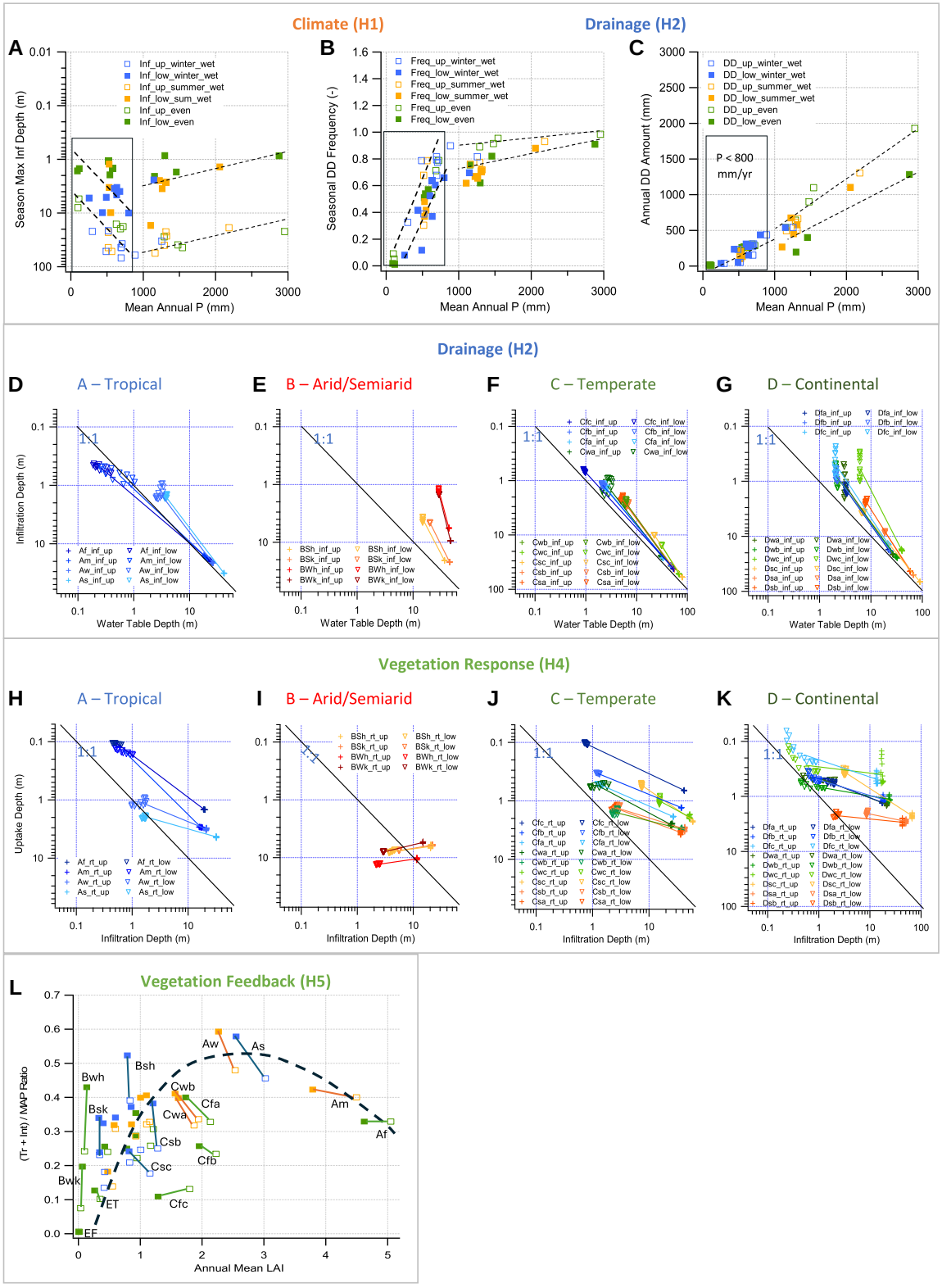

Fig. 5. Testing the hypotheses with model results. A–C) Climate (H1): *Inf*-depth, *DD* frequency and amount vs. mean annual *P*, separating uplands vs. lowlands to test H2. D–G) Drainage (H2): monthly *Inf*-depth vs. *WT*-depth in 26 climates (no polar) in four Köppen–Geiger classes, differentiating uplands (+) vs. lowlands (∇); color coding reflects annual *P*. H–K) Vegetation response (H4): mean monthly root-uptake depth vs. seasonal *Inf*-depth for the same 26 climates, in grid-cells with *LAI* > 0, separating uplands vs. lowlands. L) Vegetation feedback (H5): (*Tr* + *Int*)/*P* ratio vs. *LAI* showing the hypothesized hump-shape vegetation impact along biomass (*LAI*) gradient.

capillary rise. Here, the great root-uptake depths (5–10 m) are because *Tr* and uptake only occur in grid-cells with satellite-detectable biomass such as riparian forests, missing the widely occurring small/sparse desert plants depending on shallow local *Inf*; i.e. Fig. 5I reflects only lush riparian/oases vegetation demanding deeper water-uptake. In season-dry climates, such as in Aw

and As (Fig. 5H) and Csa and Csb (Fig. 5J), uptake depth on upland (+) terminated far above *Inf*-depth, contrary to our hypothesis. Again, the model, driven by satellite-detected, grid-cell-mean biomass, averaged out the isolated, large individual trees requiring deep uptake as shown by observations of individual plant rooting depths (Fig. 4E).

Vegetation feedback (H5)

We test H5 that vegetation water-use reinforces shallow *Inf* in dry ecosystems. The moderate correlation between root- and *Inf*-depths (Fig. 4E, Table S9, Pearson $r = 0.65$) may hint at this feedback, i.e. *Inf* cannot pass below and thus is limited by rooting-depth. We test whether this vegetation impact peaks in semiarid and season-arid climates as a hump-shaped $(Int + Tr)/P$ curve (Fig. 1D). We plot $(Int + Tr)/P$ vs. biomass, the best indicator of plant water use. Lacking consistent biomass metrics across the site-studies, we binned the reported vegetation into eight growth-form classes as proxies (Fig. 4G). Although biomass increases with higher *P* in general, it can vary widely under the same *P* (Fig. S14a) due to other factors such as terrain and land use, thus plotting $(Int + Tr)/P$ vs. biomass (instead of *P*) offers clearer insights on biomass impact. Figure 4G plots *Inf*-depth vs. biomass classes. With wide scatter, class-mean *Inf*-depths (black squares) show the expected; as biomass increases from 0 to 4, in water-limited ecosystems, higher biomass correlates with shallower *Inf*; as biomass further increases from 4 to 7, associated with increasing water surplus, higher biomass correlates with deeper *Inf*. It appears that, in the first limb, as *P* increased, $Int + Tr$ increased faster, and in the second limb, $Int + Tr$ demands are increasingly met and additional *P* can infiltrate deeper; biogenic macropores from large biomass further deepen *Inf* (35).

DD frequency/amount (Fig. S14b and c) showed no clear pattern suggesting multiple factors at play. To isolate vegetation impact on *DD*, we examine the site-studies where vegetation is the only variable across the multiple sites in the same study (Table S11). Figure 4H plots *DD* frequency vs. biomass from eight studies (45–52) and Fig. 4I plots *DD*-amount vs. biomass from 11 studies (29, 51–60). Barring two sites, they suggest declining *DD* with increasing biomass. In Carbon82 (29) (Fig. 4H), native eucalyptus–banksia (class 7, density ~580/ha) transpired less than densely planted pines (class 4, density ~1,200/ha), which transpired less than perennial pasture (class 3, sowed-grazed); in Greenwood17 (57) (Fig. 4I), native deciduous broadleaf forests (class 6) transpired less than plantation pines (class 4); both suggesting that growth forms are poor indicators of biomass of managed vegetation.

The model, driven by satellite-detected monthly biomass (*LAI*), suggests that the $(Int + Tr)/P$ ratio vs. biomass (Fig. 5L, Table S6) indeed takes the expected hump-shape (Fig. 1D), peaking in season-arid Aw (tropical, winter-dry) and As (tropical, summer-dry) and semiarid BSh climates. It supports the results of a combining field, remote-sensing, and ecohydrologic modeling study (30). Our model, simulating lateral hydrologic convergence, also shows that the ratio is higher in lowlands (filled squares, Fig. 5L) in season-arid (Aw, As), semiarid (BSh), and arid (BWh) climates, because runoff from uplands supports higher lowland biomass. Here, the valley vegetation consumes not only the local *P*, but also the *DD* from uplands (7).

Dry soil zone (H6)

We examine the climate–terrain–vegetation junctions leading to the presence/absence of a soil dry zone (Fig. 1B) that separates the modern-day surface hydrology from the deep fossil groundwater. Figure S15 shows the observed soil water profiles/fluxes at 12 sites (Table S12) at typical climate–drainage junctions, and with site-specific B-horizon (gray shade), vegetation, root-depth and *WT*-depth, and the dry soil zone (orange box; see Section S3.6 for dry-zone inference). The 12 cases, a small sample of diverse settings across the land, may highlight some key climate–terrain–vegetation interactions.

In the arid upland (case 1, Fig. S15), the dry zone is substantial and persistent (61). It thins downslope (case 2) as the *WT* becomes shallower (62) and accessible to the deep-rooted mesquite. It further thins toward the basin floor (case 3) where the *WT* provides all *Tr* for the salt cedar with 4 m deep roots (63).

In semiarid climates (second row, Fig. S15), the dry zone is highly sensitive to the vegetation, absent in the upland (case 4) under annual crops, but 2 m thick under perennial alfalfa (38). Downslope (case 5), the dry zone is absent under the bare soil and the native shrub, but present under the pines ($DD = 60\%$, 33%, 0% of *P*) with >4 m roots tapping the *WT* (53, 64). Further downslope (case 6), a dry zone appeared after a drought year (based on annual *DD*) (65).

In climates with strong rainy or melt seasons (third row, Fig. S15) wetting the regolith deeply, a dry zone is rarer but depends on the substrate. In case 7, the deep rock fractures channeled the fast/deep *Inf* to a *WT* above the fresh bedrock (18), but in case 8, the multiple Bhs-horizons (yellow bands) halted *Inf* at 7 m depth (10). In case 9, a lower site in the same study, a dry zone is absent despite a Bhs-horizon (gray) just above the *WT* (10). Here, the *WT* is within root and bioturbation reach, which breaks the barriers.

In humid climates (bottom row, Fig. S15), the dry zone is absent. In case 10, despite dry-season depletion to 6 m depth during the 5 months of $P < 100$ mm, the entire 20 m profile is replenished in the wet season ($DD \approx 30\%$ *P* (66)) (21). In case 11, the soil Bt-horizons, partially eroded by cultivation (67–69), did not prevent *Inf* from reaching the ~5 m *WT* fluctuating 4–10 m (68); river chemistry confirms this: the acidic *DD* is neutralized by weathering the igneous rock below before it is flushed to streams (6). In case 12, a Btg-horizon forms above a shallow fluctuating *WT*, but it has no impact on *DD* (70); here, as in case 9 above, a B-horizon just above a shallow *WT* is within the root and bioturbation reach.

We use the model to explore the global patterns in the dry-zone depth and thickness. Figure S16 gives the model results (showing locations of the 12 cases in Fig. S15). Consistent with site-studies, the model suggests a substantial soil dry zone in arid climates, which is absent in season-wet and wet climates, and within a climate (insets), it thins toward the valleys because of the thinner vadose zone.

Discussion

The distinct functions of hydrologic long- vs. short-circuiting prompted some basic questions: Across the land today, where does long-circuiting prevail and where is short-circuiting the norm? What forces and feedbacks create such patterns? We tested six hypotheses: (H1) at the global–regional scales, *Inf* and *DD* broadly reflect the climate; (H2) at the regional–landscape scales, *Inf* and *DD* differ from the uplands to the lowlands via mechanisms that depend on the climate; (H3) at the landscape–plot scales, the structure of the soil–saprolite–rock column exerts primary controls on *Inf* and *DD*; (H4) plant root-uptake follows *Inf* where water is limiting; (H5) plant water-uptake reduces *DD*

reinforcing shallow *Inf*; and (H6) short-circuiting creates a soil dry-zone separating the modern surface processes from the fossil groundwater.

Synthesizing site-based observations aided by a global model, we tested these hypotheses and found that: (i) Long-circuiting prevails in evenly wet climates, in well-drained landscapes with a deep vadose zone, in substrates with deep conduits, and with plant biomass below natural equilibrium. (ii) Soil B-horizons, via geochemical and vegetation feedbacks, enhance short-circuiting, while deep rock fractures enable long-circuiting even in dry climates. (iii) In dry climates/seasons and in the uplands, plant roots follow *Inf* into the deep vadose zone filled in the wet-season. (iv) Plant water-use reinforces shallow *Inf*, reducing *DD* and regolith flushing in dry and season-dry climates. (v) Where short-circuiting prevails, a dry soil zone separates the modern surface processes from the fossil groundwater. These findings, rooted in site-based process studies and scaled up to global patterns and functions, shed light on the possible global significance of specific critical zone processes discovered at plot, hillslope, and catchment scales.

To probe the implications to the Earth-system level functions, we further examine a set of modeled global maps. At the grid resolution of ∼1 km, neglecting soil B-horizons, deep rock fractures, and human impacts, these maps do not predict the actual values at specific sites but can be useful for exploring possible planetary-scale structures and functions of the Earth's critical zone arising from first-order interactions among climate, terrain, and vegetation.

Figure 3A shown earlier, the seasonal *Inf*-depth, offers a glimpse of the possible depth that is regularly moistened and aerated (above *WT*); this is the primary habitat for soil and plant life. Figure 3B and C offers the global views of *DD* frequency and amount whereby the regolith is flushed, aquifers filled, rivers fed by groundwater, but also where nutrients/pollutants are mobilized. Figure S16 gives the possible thickness of the soil dry zone, or the degree of separation between the soil and the groundwater hydrology. This dry zone severs the hydraulic and biogeochemical connections between the modern surface processes and the deep fossil groundwater replenished in the past and recording past environmental signals. It also indicates areas on Earth where the land exchanges mass/energy only with the atmosphere above, but contributes little toward freshwater and geochemical export to the oceans downstream.

Figure 6A–C offers additional views (Section S3.7). Figure 6A is the depth that supplies $E+Tr$ and latent heat to the atmosphere above, hinting at the possible subsurface depths that regulate weather, climate, and short-term carbon cycle, or the minimum depth to be considered in climate models. Far from being a fixed depth across the land, it can vary over orders of magnitude. Climate is not the only driver. For example, it is shallow in arid uplands (Sahara, point 1 on map), limited by the shallow *Inf* from low *P*, but it is also shallow in humid lowlands (Amazon floodplain, point 2), limited by the shallow *WT* due to poor drainage. For another example, it is deep in arid lowlands (Arizona–Mexico, inset 3; Tarim Bains, inset 4) where the higher valley vegetation taps the deep yet accessible *WT*, but it is also deep in season-dry uplands (eastern Brazil, inset 5) where the deep wet-season *Inf* supplies deep dry-season uptake by the large biomass, suggesting opportunistic biomass distribution and water use adapted to water availability in space-time. However, the structures in Fig. 6A arose from processes deeper than $E+Tr$ depth. For example, valley $E+Tr$ at points 3 and 4 in arid valleys is sustained by a shallow *WT*, but the latter a result of multiscale river–groundwater convergence from the high mountains to the low valleys. Where regional groundwater flow is involved, it can be tens to hundreds of kilometers in distance and tens to hundreds of meters in depth (62, 71, 72).

As the regolith flushing rate and fluid residence-time regulates the chemical weathering rates (73), we show in Fig. 6B the vertically integrated annual groundwater outflow rate, which is the sum of the lateral export to down-gradient model grid-cells plus the upward discharge into the rivers–floodplains within a grid-cell. This exit-flux can give a sense of the rigor of regolith flushing. Together with the groundwater residence times (Fig. 6C), it highlights some multiscale features relevant to chemical denudation rates of continents. Globally, climatic water budget causes stagnant flow in arid and active flow in humid climates; e.g. contrast the Sahara and the Amazon. Regionally, flushing is more active in the better-drained uplands than in the flat basin sediments; e.g. contrast the major floodplains, such as the Sudd, the Orinoco, and the North China Plain (points 6, 7, and 8 respectively, in Fig. 6B and C) to their surrounding high grounds. Finally, the major mountain ranges of the world, especially on the windward fronts, see highest flushing rates and shortest residence times, result of the high orographic *P* combined with the steep terrain, despite low mountain permeability in the model (Fig. S2); mountain flushing can be further strengthened by deep fractures due to high crustal stress in high-relief terrain (13, 74) absent in our model. The deeper *Inf* (Fig. 3A, supporting observation in (75, 76)) and the higher flushing rates in mountains suggest that mountain hydrology itself is conducive to chemical denudation besides other mechanisms such as abundance of fresh minerals (77, 78).

Our findings may also inform the discussions on the role of vegetation in chemical denudation. It is widely accepted that vegetation accelerates weathering (79) as evidenced by stream chemistry (80–82), and that enhanced silicate weathering accompanying the land-plant radiation in Devonian profoundly altered the Earth system (83–85). But if vegetation reduces *DD* and regolith flushing (H5), then its role may be double-edged. Key to elucidating this double-edged effect is to separate the weathering reactions whereby the minerals are chemically broken down, from pore-fluid flushing whereby the products are flushed into streams, as suggested by Berner (86) and Balogh-Brunstad et al. (87). The two processes are often combined into chemical denudation as their signals are often integrated in river chemistry, concealing the bottle-neck that limits denudation rates. If separated, the role of vegetation may be viewed with greater clarity. For example, in sand-box experiments (52, 87) equipped with soil samplers and lysimeters under pines, grasses, and moss-lichens, Si concentration below pines is 2× higher than below moss/lichen, but *DD* in the latter is 1.4–2.6× higher; the combined result is the reduced Si denudation under the pines to ∼1/2 of that under the moss/lichen; i.e. "vegetation may actually decrease chemical denudation from young, soil-building ecosystems" (52).

Lastly, the site-studies highlight the importance of shallow soil B-horizons and deep rock fractures. Questions remain on their global significance and ecological and geochemical consequences, and on how ecosystem predictions may change by accounting for them where they are the defining features of the substrate (17). Lacking such critical features, our model is only a crude attempt to portray the enormously complex subsurface, but it is meant to spur further thoughts and site observations strategically designed for piecing together the global structure

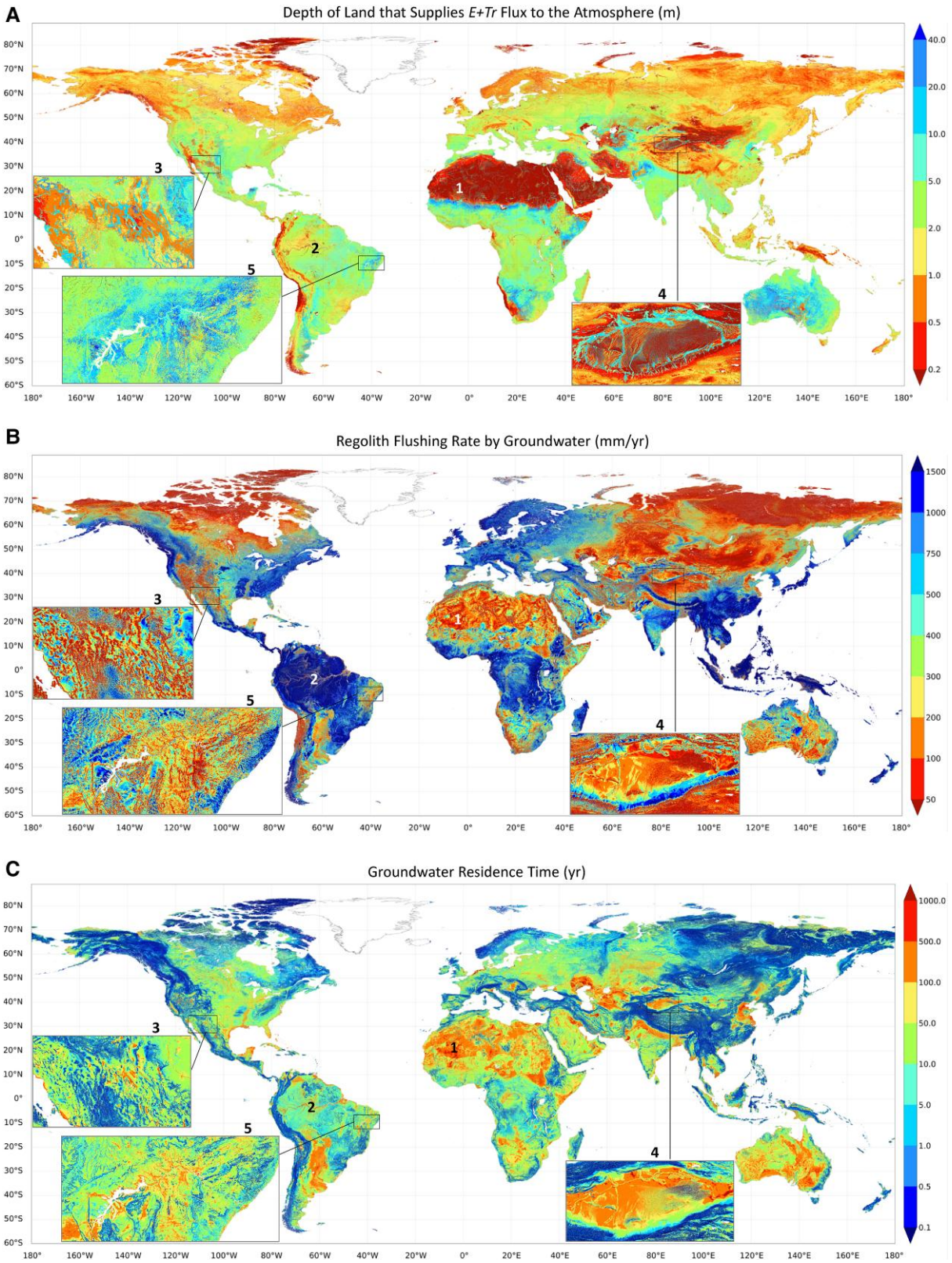

Fig. 6. A) Modeled depths of land supplying $E + Tr$ fluxes to the atmosphere (m), B) vertically integrated groundwater flushing rate (mm/year), and C) vertically averaged groundwater residence time (year).

of subsurface properties that govern water storage and flow in the Earth's critical zone. This zone, with unknown thickness, functions in capacity as the lithospheric boundary layer to the Earth's climate system, trading material and energy with the atmosphere above, and sending products of that trade to the oceans downstream. What does this zone look like today, how did it change through Earth history, and how will its functions change in the future?

Acknowledgments

The authors would like to thank the many authors of the site-studies providing observational insights, and we apologize for missing many other relevant studies.

Supplementary Material

Supplementary material is available at *PNAS Nexus* online.

Funding

This work is supported by the NSF (EAR-825813, AGS-185270) and the Spanish Ministerio de Ciencia e Innovación RIESPIRO (PID2021128510OB-I00). Computation is performed at the Supercomputing Center at Universidade de Santiago de Compostela, Galicia, Spain.

Author Contributions

Y.F. conceptulized the study and compiled site-based observations. G.M.-M. performed model simulations.

Data Availability

Site-based observations are given in Supplementary Datasheet. Global model code is shared in GitHub: https://github.com/gmiguez/MMF-HYDROMODEL. Digital files in Figs. 3 and 6 can be downloaded at: http://thredds-gfnl.usc.es/thredds/catalog/INFILTRATION_DATA/catalog.html.

References

1 Richter DD, Billings SA. 2015. 'One physical system': Tansley's ecosystem as Earth's critical zone. *New Phytol*. 206:900–912.
2 Brantley SL, *et al.* 2017. Designing a network of critical zone observatories to explore the living skin of the terrestrial Earth. *Earth Surf Dyn*. 5:841–860.
3 Grant GE, Dietrich WE. 2017. The frontier beneath our feet. *Water Resour Res*. 53:2605–2609.
4 Keller CK. 2019. Carbon exports from terrestrial ecosystems: a critical-zone framework. *Ecosystems*. 22:1691–1705.
5 Anderson RS, Rajaram H, Anderson SP. 2019. Climate driven coevolution of weathering profiles and hillslope topography generates dramatic differences in critical zone architecture. *Hydrol Process*. 33:4–19.
6 Richter DD, Markewitz D. 1995. How deep is soil? *BioScience*. 45: 600–609.
7 Miguez-Macho G, Fan Y. 2021. Spatiotemporal origin of soil water taken up by vegetation. *Nature*. 598:624–628.
8 Fan Y, Duffy CJ, Oliver DS. 1997. Density-driven groundwater flow in closed desert basins: field investigations and numerical experiments. *J Hydrol*. 196:139–184.
9 Zhou H, Zhao WZ, Yang QY. 2016. Root biomass distribution of planted *Haloxylon ammodendron* in a duplex soil in an oasis: desert boundary area. *Ecol Res*. 31:673–681.
10 Strobach E, Harris BD, Dupuis JC, Kepic AW. 2014. Time-lapse borehole radar for monitoring rainfall infiltration through podosol horizons in a sandy vadose zone. *Water Resour Res*. 50: 2140–2163.
11 Smith TJ, *et al.* 2011. Small soil storage capacity limits benefit of winter snowpack to upland vegetation. *Hydrol Process*. 25: 3858–3865.
12 Bales RC, *et al.* 2011. Soil moisture response to snowmelt and rainfall in a Sierra Nevada mixed-conifer forest. *Vadose Zone J*. 10:786–799.
13 St. Clair J, *et al.* 2015. Geophysical imaging reveals topographic stress control of bedrock weathering. *Science*. 350:534–538.
14 Molnar P, Anderson RS, Anderson SP. 2007. Tectonics, fracturing of rock, and erosion. *J Geophys Res Earth Surf*. 112:12. https://doi.org/10.1029/2005JF000433
15 Arbel Y, Greenbaum N, Lange J, Inbar M. 2010. Infiltration processes and flow rates in developed karst vadose zone using tracers in cave drips. *Earth Surf Proc Land*. 35:1682–1693.
16 Salve R, Rempe DM, Dietrich WE. 2012. Rain, rock moisture dynamics, and the rapid response of perched groundwater in weathered, fractured argillite underlying a steep hillslope. *Water Resour Res*. 48(11). doi:10.1029/2012WR012583.
17 Hahm WJ, *et al.* 2019. Lithologically controlled subsurface critical zone thickness and water storage capacity determine regional plant community composition. *Water Resour Res*. 55:3028–3055.
18 Rempe DM, Dietrich WE. 2018. Direct observations of rock moisture, a hidden component of the hydrologic cycle. *Proc Natl Acad Sci U S A*. 115:2664–2669.
19 van Schaik NLMB, Schnabel S, Jetten VG. 2008. The influence of preferential flow on hillslope hydrology in a semi-arid watershed (in the Spanish Dehesas). *Hydrol Process*. 22:3844–3855.
20 Nativ R, Adar E, Dahan O, Geyh M. 1995. Water recharge and solute transport through the vadose zone of fractured chalk under desert conditions. *Water Resour Res*. 31:253–261.
21 Davidson E, *et al.* 2011. Carbon inputs and water uptake in deep soils of an Eastern Amazon forest. *Forest Sci*. 57:51–58.
22 Cannon WA. 1911. *The root habits of desert plants*. Carnegie Institution of Washington. p. 156.
23 Sturges DL. 1977. Soil water withdrawal and root characteristics of big sagebrush. *Am Midl Nat*. 98:257–274.
24 McCormick EL, *et al.* 2021. Widespread woody plant use of water stored in bedrock. *Nature*. 597:225–229.
25 Sala OE, Lauenroth WK. 1982. Small rainfall events—an ecological role in semi-arid regions. *Oecologia*. 53:301–304.
26 Giehl RF, von Wirén N. 2014. Root nutrient foraging. *Plant Physiol*. 166:509–517.
27 Fan Y, Miguez-Macho G, Jobbagy EG, Jackson RB, Otero-Casal C. 2017. Hydrologic regulation of plant rooting depth. *Proc Natl Acad Sci U S A*. 114:10572–10577.
28 Bunger MT, Thomson HJ. 1938. Root development as a factor in the success or failure of windbreak trees in the southern High Plains. *J For*. 36:790–803. https://doi.org/10.1093/jof/36.8.790
29 Carbon BA, Roberts FJ, Farrington P, Beresford JD. 1982. Deep drainage and water use of forests and pastures grown on deep sands in a Mediterranean environment. *J Hydrol*. 55:53–63.
30 Good SP, Moore GW, Miralles DG. 2017. A mesic maximum in biological water use demarcates biome sensitivity to aridity shifts. *Nat Ecol Evol*. 1:1883–1888.
31 Galle S, Ehrmann M, Peugeot C. 1999. Water balance in a banded vegetation pattern—a case study of tiger bush in western Niger. *Catena (Amst)*. 37:197–216.
32 Rossi MJ, *et al.* 2018. Vegetation and terrain drivers of infiltration depth along a semiarid hillslope. *Sci Total Environ*. 644:1399–1408.
33 Glover PE, Glover J, Gwynne MD. 1962. Light rainfall and plant-survival in E-Africa II. Dry grassland vegetation. *J Ecol*. 50:199.
34 Puigdefabregas J. 2005. The role of vegetation patterns in structuring runoff and sediment fluxes in drylands. *Earth Surf Proc Land*. 30:133–147.

35 Liang WL, Kosugi K, Mizuyama T. 2007. Heterogeneous soil water dynamics around a tree growing on a steep hillslope. *Vadose Zone J*. 6:879–889.

36 Nulsen RA, Bligh KJ, Baxter IN, Solin EJ, Imrie DH. 1986. The fate of rainfall in a mallee and heath vegetated catchment in Southern Western Australia. *Aust J Ecol*. 11:361–371.

37 Qiao L, Zou CB, Stebler E, Will RE. 2017. Woody plant encroachment reduces annual runoff and shifts runoff mechanisms in the tallgrass prairie, USA. *Water Resour Res*. 53:4838–4849.

38 Fu X, Shao M, Wei X, Wang H, Zeng C. 2013. Effects of monovegetation restoration types on soil water distribution and balance on a hillslope in northern Loess Plateau of China. *J Hydrol Eng*. 18: 413–421.

39 Yan WM, Deng L, Zhong YQW, Shangguan ZP. 2015. The characters of dry soil layer on the Loess Plateau in China and their influencing factors. *PLoS One*. 10:e0134902.

40 Fan Y, Li H, Miguez-Macho G. 2013. Global patterns of groundwater table depth. *Science*. 339:940–943.

41 Fan Y, Miguez-Macho G. 2011. A simple hydrologic framework for simulating wetlands in climate and earth system models. *Clim Dyn*. 37:253–278.

42 Pastorello G, *et al*. 2020. The FLUXNET2015 dataset and the ONEFlux processing pipeline for eddy covariance data. *Sci Data*. 7:225.

43 Skrzypek G, Dogramaci S, Page GFM, Rouillard A, Grierson PF. 2019. Unique stable isotope signatures of large cyclonic events as a tracer of soil moisture dynamics in the semiarid subtropics. *J Hydrol*. 578:124124.

44 Taylor RG, *et al*. 2013. Evidence of the dependence of groundwater resources on extreme rainfall in East Africa. *Nat Clim Change*. 3:374–378.

45 Zhao M, *et al*. 2021. Soil water dynamics based on a contrastive experiment between vegetated and non-vegetated sites in a semiarid region in Northwest China. *J Hydrol*. 603:126880.

46 Fan J, Wang Q, Jones SB, Shao M. 2016. Soil water depletion and recharge under different land cover in China's Loess Plateau. *Ecohydrology*. 9:396–406.

47 Ke H, Li P, Li Z, Shi P, Hou J. 2019. Soil water movement changes associated with revegetation on the Loess Plateau of China. *Water (Basel)*. 11:731.

48 Ramier D, *et al*. 2009. Towards an understanding of coupled physical and biological processes in the cultivated Sahel—1. Energy and water. *J Hydrol*. 375:204–216.

49 Lyne Ensign K, Webb EA, Longstaffe FJ. 2006. Microenvironmental and seasonal variations in soil water content of the unsaturated zone of a sand dune system at Pinery Provincial Park, Ontario, Canada. *Geoderma*. 136:788–802.

50 Gardner R, McLaren S. 1999. Infiltration and moisture movement in coastal sand dunes, Studland, Dorset. U.K.: preliminary results. *J Coast Res*. 15:936–949.

51 Oliveira PTS, *et al*. 2017. Groundwater recharge decrease with increased vegetation density in the Brazilian Cerrado. *Ecohydrology*. 10:e1759.

52 O'Brien R, Keller CK, Strobridge DM. 2004. Plant-cover effects on hydrology and pedogenesis in a sandy vadose zone. *Geoderma*. 118:63–76.

53 Cheng Y, *et al*. 2020. New measures of deep soil water recharge during the vegetation restoration process in semi-arid regions of northern China. *Hydrol Earth Syst Sci*. 24:5875–5890.

54 Jayawickreme DH, Santoni CS, Kim JH, Jobbágy EG, Jackson RB. 2011. Changes in hydrology and salinity accompanying a century of agricultural conversion in Argentina. *Ecol Appl*. 21:2367–2379.

55 Green JC, Reid I, Calder IR, Nisbet TR. 2006. Four-year comparison of water contents beneath a grass ley and a deciduous oak wood overlying Triassic sandstone in lowland England. *J Hydrol*. 329: 16–25.

56 Weltz MA, Blackburn WH. 1995. Water budget for south Texas rangelands. *J Range Manage*. 48:45–52.

57 Greenwood WJ, Buttle JM. 2018. Land cover controls on depression-focused recharge on the Oak Ridges Moraine, Southern Ontario, Canada. *Hydrol Process*. 32:1909–1926.

58 Rodrigues Capítulo L, Carretero SC, Kruse EE. 2018. Impact of afforestation on coastal aquifer recharge. Case study: eastern coast of the province of Buenos Aires, Argentina. *Environ Earth Sci*. 77:74.

59 Nosetto MD, Jobbágy EG, Brizuela AB, Jackson RB. 2012. The hydrologic consequences of land cover change in central Argentina. *Agric Ecosyst Environ*. 154:2–11.

60 Jipp PH, Nepstad DC, Cassel DK, Reis De Carvalho C. 1998. Deep soil moisture storage and transpiration in forests and pastures of seasonally-dry Amazonia. *Clim Change*. 39:395–412.

61 Kidron GJ. 2014. Do mosses serve as sink for rain in the Negev Desert? A theoretical and experimental approach. *Catena (Amst)*. 121:31–39.

62 Jobbágy EG, Nosetto MD, Villagra PE, Jackson RB. 2011. Water subsidies from mountains to deserts: their role in sustaining groundwater-fed oases in a sandy landscape. *Ecol Appl*. 21:678–694.

63 Wang T-Y, *et al*. 2019. Estimating groundwater evapotranspiration by phreatophytes using combined water level and soil moisture observations. *Ecohydrology*. 12:e2092.

64 Cheng Y, *et al*. 2021. On change of soil moisture distribution with vegetation reconstruction in Mu Us sandy land of China, with newly designed lysimeter. *Front Plant Sci*. 12:609529.

65 Schuh WM, Meyer RF, Sweeney MD, Gardner JC. 1993. Spatial variation of root-zone and shallow vadose-zone drainage on a loamy glacial till in a sub-humid climate. *J Hydrol*. 148:1–26.

66 Markewitz D, Devine S, Davidson EA, Brando P, Nepstad DC. 2010. Soil moisture depletion under simulated drought in the Amazon: impacts on deep root uptake. *New Phytol*. 187:592–607.

67 Austin JC, Brecheisen ZS, Cook CW, Richter DD. CCZO—soil moisture—hydroprobe—Calhoun critical zone observatory—(2016-ongoing). [accessed 2023 Nov 10]. http://www.hydroshare.org/resource/9b7328ab4c914676891fbb8ff65d98c2.

68 Mallard J, McGlynn BL. CCZO—Groundwater Depth, Electrical Conductivity—Calhoun 70-m deep well—(2014–2017). HydroShare. [accessed 2023 Nov 10]. http://www.hydroshare.org/resource/35301f29f15547c884c847ff00eb6220.

69 Heine PR. CCZO—soil texture—Calhoun CZO—(2015–2016. HydroShare. [last accessed 2023 Nov 10]. http://www.hydroshare.org/resource/1bd22f9415d3461b86f4cf3874e2e1c1.

70 Hollinger SE, Reinke BC, Peppler RA. 1994. Illinois climate network: site descriptions, instrumentation, and data management. In: Illinois State Water Survey, editors. *Illinois State water survey circular 178*. Champaign (IL): Illinois State Water Survey. p. 63.

71 Markovich KH, Manning AH, Condon LE, McIntosh JC. 2019. Mountain-block recharge: a review of current understanding. *Water Resour Res*. 55:8278–8304.

72 Fan Y. 2019. Are catchments leaky? *WIREs Water*. 6:e1386.

73 Maher K, Chamberlain CP. 2014. Hydrologic regulation of chemical weathering and the geologic carbon cycle. *Science*. 343:1502–1504.

74 Heidbach O, *et al*. 2010. Global crustal stress pattern based on the World Stress Map database release 2008. *Tectonophysics*. 482: 3–15.

75 Jasechko S, Kirchner JW, Welker JM, McDonnell JJ. 2016. Substantial proportion of global streamflow less than three months old. *Nat Geosci*. 9:126–129.

76 McIntosh JF. 2021. Grant, deep meteoric water circulation in earth's crust. *Geophys Res Lett*. 48:e2020GL090461.

77 Raymo ME, Ruddiman WF. 1992. Tectonic forcing of late Cenozoic climate. *Nature*. 359:117–122.
78 Anderson SP, Von Blanckenburg F, White AF. 2007. Physical and chemical controls on the critical zone. *Elements*. 3:315–319.
79 Drever JI. 1994. The effect of land plants on weathering rates of silicate minerals. *Geochim Cosmochim Acta*. 58:2325–2332.
80 Moulton KL, West J, Berner RA. 2000. Solute flux and mineral mass balance approaches to the quantification of plant effects on silicate weathering. *Am J Sci*. 300:539–570.
81 Pawlik Ł, Phillips JD, Šamonil P. 2016. Roots, rock, and regolith: biomechanical and biochemical weathering by trees and its impact on hillslopes—a critical literature review. *Earth Sci Rev*. 159:142–159.
82 Brantley SL, *et al*. 2017. Reviews and syntheses: on the roles trees play in building and plumbing the critical zone. *Biogeosciences*. 14:5115–5142.
83 Algeo TJ, Scheckler SE. 1998. Terrestrial-marine teleconnections in the Devonian: links between the evolution of land plants, weathering processes, and marine anoxic events. *Philos Trans R Soc B*. 353:113–130.
84 Berner RA. 1997. The rise of plants and their effect on weathering and atmospheric CO_2. *Science*. 276:544–546.
85 Dahl TW, Arens SKM. 2020. The impacts of land plant evolution on Earth's climate and oxygenation state—an interdisciplinary review. *Chem Geol*. 547:119665.
86 Berner RA. 1978. Rate control of mineral dissolution under Earth surface conditions. *Am J Sci*. 278:1235–1252.
87 Balogh-Brunstad Z, *et al*. 2008. Chemical weathering and chemical denudation dynamics through ecosystem development and disturbance. *Glob Biogeochem Cycles*. 22(1). doi:10.1029/2007GB002957.